Elongational Flow-Induced Crystallization and Structure Development in Supercooled Poly(ethylene naphthalate)†

Masami Okamoto, Hiroshi Kubo,‡ and Tadao Kotaka*

Toyota Technological Institute, Hisakata 2-12-1, Tempaku, Nagoya 468-8511, Japan

Received November 20, 1997; Revised Manuscript Received February 27, 1998

ABSTRACT: Elongational flow-induced crystallization behavior was investigated on supercooled liquids of two poly(ethylene naphthalate)s (PENs) with different crystallization habits via elongational flow optorheometry (EFOR), temperature-modulated differential scanning calorimetry (TMDSC), and Rayleigh scattering in the temperature range 170−190 °C. The samples were an antimony-catalyzed PEN (Sb-PEN) with a rapid crystallization rate but less well-organized spherulites and a germanium-catalyzed PEN (Ge-PEN) with a temperature sensitive (slow) crystallization rate but better organized spherulites. In the elongation of Sb-PEN at 170 °C, a strong tendency of *strain hardening* was observed in the early stage and transformation of the spherulites into rodlike morphology occurred in the later stage, accompanying a substantial increase in birefringence. On the other hand, for Ge-PEN at 170 °C, molecular orientation along the flow direction proceeded and flow-induced crystallization took place rather suddenly at a Hencky strain of $\epsilon \approx 2.65$, with the crystalline lamellae irregularly growing transverse to the oriented chains. However, in Ge-PEN elongated at 190 °C, especially with a low strain rate $\dot{\epsilon}_0$ (<0.01 s^{-1}), stable spherulites were formed and their growth dominated the subsequent elongation behavior. In these PENs, the features of the flow-induced structure development were governed by the dimensionless strain rate, which was the ratio of $\dot{\epsilon}_0$ to the spherulite growth rate under the quiescent state. Depending on the dimensionless strain rate being above or below the critical value, either the oriented-crystallite formation or the spherulite growth dominated the elongation behavior, respectively.

Introduction

Flow-induced structure formation in a polymeric liquid under elongation involves orientation of the polymer chains and the subsequent crystallization and/or deformation of the already existing spherulites. It is thus important to understand the elongational flow-induced structure development behavior in various semicrystalline polymers under a supercooled liquid state for the optimization of their processing strategies such as blow molding and film processing.

In our previous papers,[1−4] we discussed results of rheological[2] and structural studies[3,4] on supercooled liquids of poly(ethylene terephthalate)s (PETs) under elongation via elongational flow optorheometry (EFOR), which enabled us to simultaneously measurement transient tensile stresses and birefringence under uniaxial elongation with constant Hencky strain rates,[1] temperature-modulated differential scanning calorimetry[2] (TMDSC), and Rayleigh scattering[3,4] in the temperature range 100−130 °C that was comparable to the blow-molding and/or film-blowing conditions for PET.[5−7]

Poly(ethylene naphthalate) (PEN) is also a semicrystalline polyester possessing naphtalene rings in the main chain, which provide rigidity, resulting in the higher glass transition temperature T_g (∼120 °C) and melting point T_m (=268 °C) as well as the higher modulus and lower creep compliance as compared to those for PET.[8,9]

Recently, using a time-resolved X-ray diffraction apparatus equipped with an imaging plate system, Murakami et al.[10,11] reported that, in the uniaxial free-width drawing of an unoriented amorphous PEN film in the temperature range 130−150 °C, the naphthalene rings were preferentially aligned parallel to the film surface during the necking process. Above 160 °C, on the other hand, the PEN film was stretched uniformly and the necking behavior was not observed. However, there remain many other unsolved problems before the full elucidation of its orientational crystallization behavior under drawing, especially in elongational flow under the supercooled liquid state.

In this paper, we examined the flow-induced crystallization behavior of PENs with different crystallization habits. Specifically we used PEN resins catalyzed with germanium (Ge) or antimony (Sb), both of which were commonly used in practical processing operations. Under a quiescent state (between T_g and T_m) the former (Ge-PEN) crystallizes slowly, but the latter (Sb-PEN) crystallizes quickly, just as is known for Ge-PET and Sb-PET.[4,12] Such a comparison is thus worthwhile for studying the features of transformation of the crystalline textures under elongation: Depending on the flow conditions, spherulites existing before the elongation or even formed in the very early stage may transform into a new texture involving an oriented crystalline form. Such a knowledge of their elongational flow behavior should also be useful for assessing the performance of different PENs in their processing operations.

Experimental Section

Materials. A commercial poly(ethylene naphthalate) (Sb-PEN) sample of film-blowing grade polymerized with an antimony catalyst system was supplied by Teijin Ltd. To compare the effects of different crystallization habits on the elongational flow behavior, we also tested a slowly crystallizing PEN (Ge-PEN) polymerized with a germanium catalyst system supplied also by Teijin Ltd. The characteristics of both Sb-PEN and Ge-PEN resins are listed in Table 1 together with a brief description of their crystallization habits. The details will be presented in the Results (see Figures 2−5).

† Elongational Flow Optorheometry for Polymeric Liquids. Part 7.

* To whom correspondence should be addressed.

‡ Toyoda Boshoku Co., 1-1 Toyoda-cho, Kariya 448-, Japan.

S0024-9297(97)01713-0 CCC: $15.00
Published on Web 05/30/1998

Table 1. Characteristics of the PEN Resins Used in This Study

code	Sb-PEN	Ge-PEN
catalyst used	Sb	Ge
$[\eta]^a$ (dL·g^{-1})	0.71	0.71
T_g/°C	∼120	∼120
T_m/°C	269	266
$1/\tau_{1/2}{}^b$ ($\times 10^{-4}$ s^{-1})	40.0	0.56
spherulite morphology[c]	less-ordered	well-ordered
$\chi_c{}^d$ (wt %)	54.1	43.1

[a] Furnished by Teijin Ltd. Determined in a mixed solvent of *p*-chlorophenol and tetrachloroethane (7/3 v/v) at 30 °C. [b] Overall crystallization rate at 170 °C (see Figure 11). [c] See Figures 2 and 3. [d] The degree of % crystallinity under isothermal crystallization at 170 °C for 1 h (Sb-PEN) and for 10 h (Ge-PEN) estimated by TMDSC.

EFOR Run. The apparatus we employed for the present study is a combination of a Meissner's new elongational rheometer of gas-cushion type[13] commercialized as a Rheometrics melt elongational rheometer (RME, Rheometric Scientific) and a birefringence apparatus of reflection double-beam path type. We call this modified version of the RME an elongational flow optorheometer (EFOR),[1] which enabled us to carry out simultaneous measurements of transient tensile stress $\sigma(t)$ and birefringence $\Delta n(t)$ as a function of time t under a constant tensile strain rate $\dot{\epsilon}_0$.[1] The details were described elsewhere.[1]

For the EFOR tests, PEN pellets were dried at 140 °C for 16 h under a reduced pressure of 10^{-4} Torr to remove moisture before they were subjected to compression molding. The pellets were sandwiched between polyimide films (Kapton HN, Toray-DuPont) and compression-molded with a laboratory hot press kept at 300 °C ($> T_m$ of PEN) for 90 s. The molded sheet was quickly quenched to room temperature by sandwiching it with glass plates to obtain an amorphous sheet, which was then cut into strips of approximately 60 × 7.0 × 0.3 mm^3 in size and later subjected to EFOR measurements with annealing for 90 s before starting the run. The temperature range was 170−190 °C.

TMDSC Run. The glass transition T_g and melting temperatures T_m were determined on a temperature-modulated differential scanning calorimeter (TMDSC: MDSC, TA2920, TA Instruments) at a heating rate of 2 °C/min with a heating/cooling cycle of the modulation period of 60 s and an amplitude of ±0.2 °C. The principles and procedures of TMDSC can be found in literature by, for example, Wunderlick,[14] so we do not recount them here. A brief description of TMDSC applied to PET was described elsewhere.[2]

To estimate the true degrees of crystallinity χ_c present in the elongated specimens before they were subjected to the DSC test, we have to subtract the extra heat due to the crystallites being formed during the heating process of DSC from the total endothermic heat flow due to the crystalline melting. On the TMDSC run shown in Figure 1, the endothermic heat flow ΔH_{diff} for the initially existing crystallites can be easily calculated as $\Delta H_{diff} = \Delta H_{rev} - \Delta H_{nonrev}$, where ΔH_{rev} is the endothermic melting (reversing) enthalpy from the reversing heat flow profile and ΔH_{nonrev} is the exothermic ordering/crystallization (nonreversing) enthalpy from the nonreversing heat flow profile appearing in the temperature range 145−280 °C. In this particular run, the observed enthalpies were $\Delta H_{rev} = 46.7$ J/g and $\Delta H_{nonrev} = 25.2$ J/g. The χ_c was thus calculated as $\chi_c = \Delta H_{diff}/\Delta H° = 20.5\%$ with $\Delta H° = 103.4$ J/g being the melting enthalpy of 100% crystalline PEN.[15]

Optical Microscopy and Rayleigh Scattering Photometry. Then we observed the spherulite growth rate of Ge-PEN under a quiescent state in the temperature range 170−190 °C using a polarizing optical microscope (Nikon OPTI-PHOTO2-POL) equipped with a thermostated hot stage (Linkam LK600PM, Linkam Scientific Instruments, Ltd.). The details were described in our previous paper for PET.[2] For Sb-PEN, we tried to make the same observation with the optical microscope, but we could not do it because the growing spherulites of less-ordered, imperfect shape filled up the field of the microscope extremely rapidly so that we could not follow the growth of an individual spherulite, just as in the case of Sb-PET reported previously.[4]

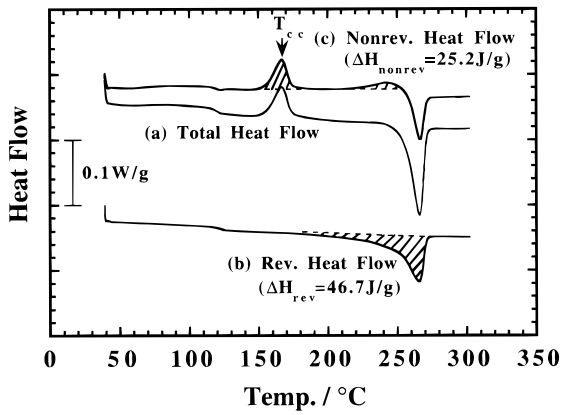

Figure 1. TMDSC scan for Ge-PEN elongated up to $\epsilon = 2.6$ with $\dot{\epsilon}_0 = 0.03$ s^{-1} at 170 °C: (a) total heat flow; (b) reversing heat flow; (c) nonreversing heat flow.

To avoid this difficulty, we employed time-resolved light scattering (LS) photometry, which is a powerful tool for estimating the overall crystallization rate and its kinetics in supercooled crystalline polymer liquids.[16,17] The LS photometer was equipped with a 38-channel photodiode array (PDA: Hamamastu Photonics Co.), which facilitated time-resolved measurement of LS profiles (the angular dependence of scattered light intensity) with a time slice of 1/30 s. The position of the PDA was adjusted by sliding its holder from 20 to 600 mm distance so that the scattering angles of 1.4−30 were covered. We observed changes of LS profiles with time after the temperature drop at an appropriate interval of usually 1−50 s. A plane polarized light from a He−Ne laser of 632.8-nm wavelength was applied vertically to the specimen, and the scattering profile was observed at an azimuthal angle of 45° under Hv (cross-polarized) optical alignment.

To analyze the scattering data, we employed the integrated scattering intensity, that is, the invariant Q defined by

$$Q = \int_0^\infty I(q) q^2 \, dq \tag{1a}$$

$$q = (4\pi/\lambda) \sin(\theta/2) \tag{1b}$$

where q is the scattering vector corresponding to the scattering angle θ as defined in eq 1b, λ is the wavelength of light in the specimen, and I(q) is the intensity of the scattered light at q.[16]

In the course of the spherulite growth or isothermal crystallization under a quiescent state, scattering intensity increases with time, reflecting the increase in optical anisotropy caused by the crystallization. Then the invariant Q for the Hv mode is essentially Q_δ, corresponding to the mean-square optical anisotropy $\langle\delta^2\rangle$, defined as

$$Q_\delta \propto \langle\delta^2\rangle \propto \phi_s(\alpha_r - \alpha_t)^2 \tag{2}$$

where ϕ_s is the volume fraction of the spherulites and α_r and α_t are the radial and tangental polarizabilities of the spherulites, respectively.[18] We constructed a plot of reduced invariant $Q_\delta/Q_\delta{}^\infty$ versus time t with $Q_\delta{}^\infty$ being Q_δ at an infinitely long time, where the crystallization had been completed. It was in fact ∼10 h for the present experiments. Then taking the *crystallization half-time* $\tau_{1/2}$, at which $Q_\delta/Q_\delta{}^\infty$ reaches $^1/_2$, we defined $1/\tau_{1/2}$ as a measure of the overall crystallization rate.

For LS measurements under a quiescent state,[16,17] dried PEN pellets were sandwiched between two pieces of cover glass, placed on a laboratory hot press, and compression molded at 300 °C for 90 s to obtain a thin film ∼30 μm thick. The molten film was rapidly quenched to a prescribed supercooled state between 170 and 190 °C by putting it on the

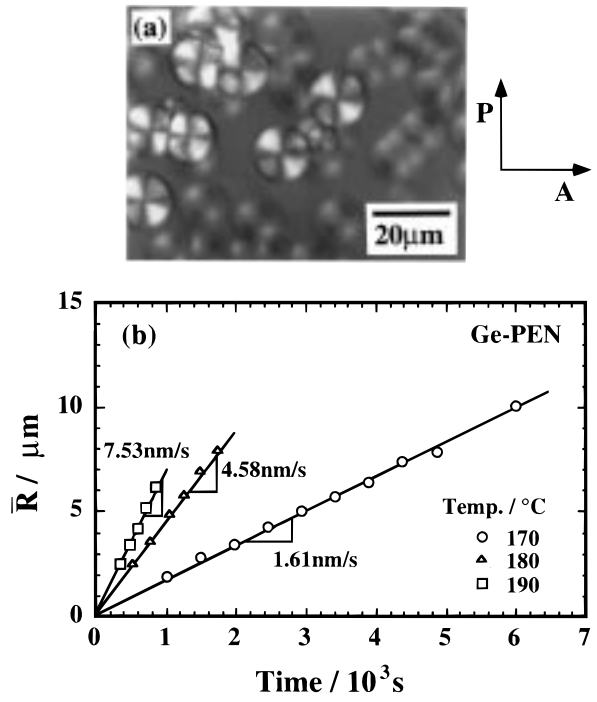

Figure 2. Spherulite growth of Ge-PEN under the quiescent state during isothermal crystallization: (a) polarized optical micrograph for 4800 s at 170 °C and (b) time variation of the radii of the spherulites at various temperatures between 170 and 190 °C.

thermostated hot-stage set on the LS apparatus. Immediately after the temperature drop, time-resolved LS measurement was carried out, as described in the previous articles.[16,17]

We also applied the LS photometry to specimens subjected to EFOR to see the elongational flow-induced crystallization behavior. To this end, we conducted an *ex situ* measurement, in which a test specimen subjected to EFOR to a certain extent of elongation $\epsilon(t)$ was taken out and quickly quenched by sandwiching it between cold metal plates to freeze the internal structure developed during the elongation. Then the center portion of the specimen ~40−200 μm thick (depending on the extent of $\epsilon(t)$) was cut out and held between cover glasses to avoid the diffuse surface. The scattering profile under Hv (cross-polarized) optical alignment was monitored with the photodiode array and also recorded whenever necessary on a photographic film (Fuji FP-100B; ISO = 100) with an exposure time of 1 to $^1/_4$ s.

Results

Rayleigh Scattering Photometry under the Quiescent State. Figure 2a shows a typical example of a polarized micrograph for a developed spherulite under isothermal crystallization after 4800 s at 170 °C. Figure 2b shows the time t variation of the radii $\bar{R}$ for Ge-PEN at various supercooled states. A linear increase in $\bar{R}$ passing through the origin is seen in a wide range of the time scale. The result implies that the volume fraction increases in proportion to t^3. Note that spherulite growth occurs immediately after the temperature drop with zero induction time. The fact suggests that heterogeneous nucleation proceeded in a manner similar to that for the PET case.[2,19,20] Within the range 170−190 °C, the growth rate for Ge-PEN defined as the initial slope of the $\bar{R}$ versus t relation (=d$\bar{R}$/dt) increases with increasing crystallization temperature. At 190 °C the rate is as much as 5 times faster than that at 170 °C.

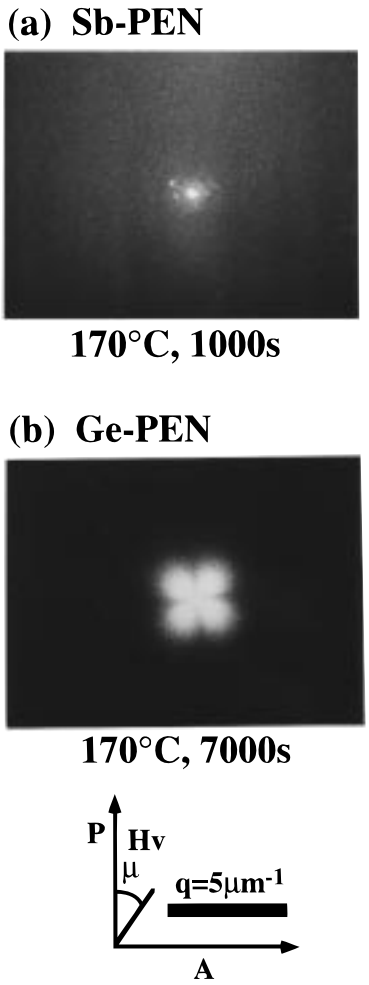

Figure 3. Hv light-scattering patterns of (a) Sb- and (b) Ge-PEN obtained under isothermal crystallization at 170 °C.

On the other hand, Sb-PEN has a too rapid overall-crystallization rate, so that we can hardly follow the spherulite growth under a polarizing optical microscope. We thus employed for Sb-PEN time-resolved LS photometry. Figure 3 shows typical examples of LS Hv patterns for (a) Sb-PEN taken at 170 °C after a sufficiently long time (~1000 s), by which time the spherulite growth had been completed and the spherulites covered all the field of the microscope. For comparison, Figure 3b shows an LS profile for Ge-PEN after 7000 s of crystallization at 170 °C. In Figure 3a for Sb-PEN, a large smeared isotropic pattern is observed, indicating formation of a large number of less well-organized spherulites. For Sb-PEN the locations and intensities of the scattering maxima along the azimuthal angle μ are not quite clear even in such a late-stage crystallization. We thus could not follow the time evolution of the peak angles and intensities, from which the average spherulite size was usually estimated. On the other hand, in Figure 3b for Ge-PEN, a four-leaf-clover pattern typical to well-developed spherulites is seen.

Figure 4 shows the time variation of the reduced invariant Q_δ/Q_δ^∞ taken for Ge-PEN at three different temperatures from 170 to 190 °C and for Sb-PEN at 170 °C. From the slope $(\partial(Q_\delta/Q_\delta^\infty)/\partial t)_T$ at the *crystallization half-time* of these curves, we estimated the spherulite growth rate, and we plotted it in Figure 5 against

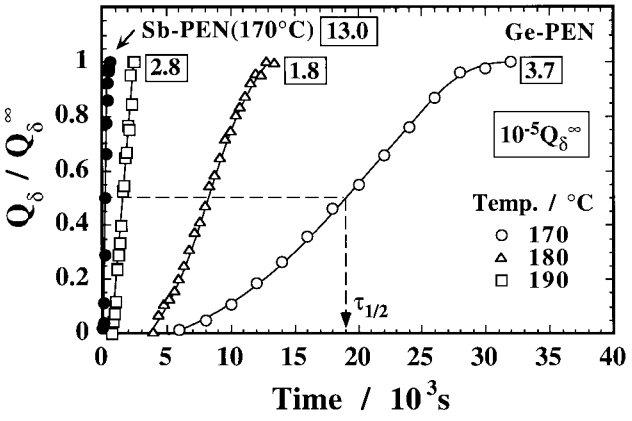

Figure 4. Time variation of reduced invariant Q_δ/Q_δ^∞ during isothermal crystallization at the quiescent state in the temperature range from 170 to 190 °C for Ge-PEN and at 170 °C for Sb-PEN. The arrow indicates the *crystallization half-time* $\tau_{1/2}$ for 170 °C. The values of Q_δ^∞ of each specimen were shown with the number in the box.

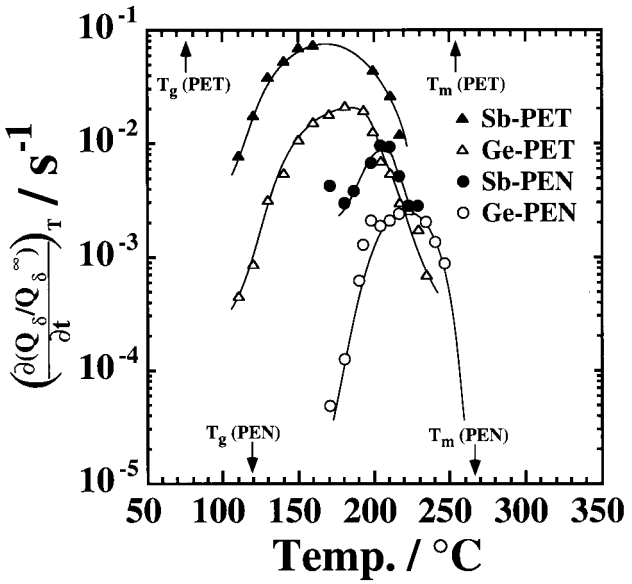

Figure 5. Temperature dependence of overall crystallization rate $(\partial(Q_\delta/Q_\delta^\infty)/\partial t)_T$ for Sb- and Ge-PEN with those of PETs data for comparison (refs 2 and 3).

temperature. For comparison, similar plots for PETs[3,4] are also included in the same figure.

Elongational Viscosity. We then attempted to determine the transient tensile stress $\sigma(\dot\epsilon_0;t)$ and the elongational viscosity $\eta_E(\dot\epsilon_0;t)$ ($\equiv\sigma(\dot\epsilon_0;t)/\dot\epsilon_0$) for PENs as a function of the Hencky strain rate $\dot\epsilon_0$ and time t on EFOR in the temperature range between 170 and 190 °C covered in the isothermal crystallization experiments. However, above 180 °C, Sb-PEN crystallized so fast that the specimen became tough and slipped between the metal belt clamps of EFOR so that we could not precisely determine $\sigma(\dot\epsilon_0;t)$ and $\eta_E(\dot\epsilon_0;t)$. Thus for Sb-PEN we collected data only at 170 °C, where the spherulite growth was moderate. Figures 6 and 7 show respectively the results for Ge-PEN and Sb-PEN. The arrows in the figures show the critical (*up-rising*) time t_{η_E} at which upward deviation from the $\dot\epsilon_0$-independent portion of the $\eta_E(\dot\epsilon_0;t)$ curves becomes prevailing. We call the $\dot\epsilon_0$-independent portion the *linear* portion and the deviation the tendency of *strain-induced hardening*.

In Figure 8 we plotted the critical (up-rising) Hencky strain ϵ_{η_E} ($\equiv\dot\epsilon_0 t_{\eta_E}$) against the Hencky strain rate $\dot\epsilon_0$ for

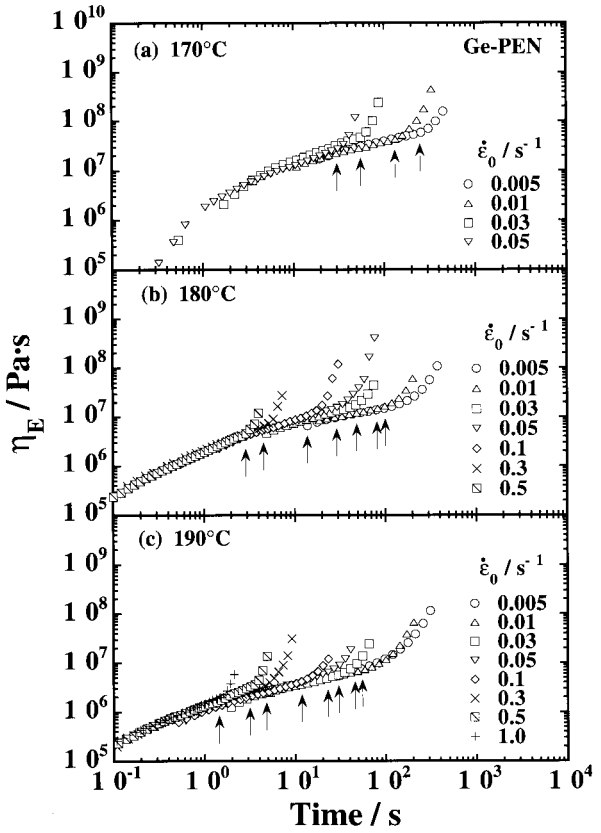

Figure 6. Time variation of elongational viscosity $\eta_E(\dot\epsilon_0;t)$ for Ge-PEN in various supercooled states with various $\dot\epsilon_0$ values from 0.005 to 1.0 s^{-1}. The arrows indicate the *up-rising* time τ_{η_E} at which $\eta_E(t)$ begins to deviate from the linear, $\dot\epsilon_0$-independent $\eta_E(t)$ versus t curves.

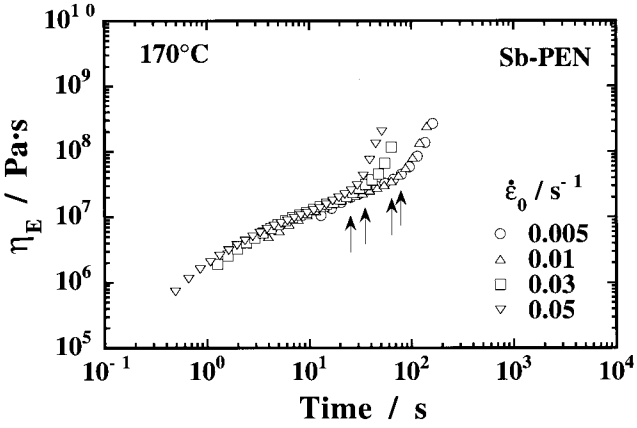

Figure 7. Time variation of elongational viscosity $\eta_E(\dot\epsilon_0;t)$ for Sb-PEN in various supercooled states with various $\dot\epsilon_0$ values from 0.005 to 0.05 s^{-1}. The arrows indicate the *up-rising* time t_{η_E} at which $\eta_E(t)$ begins to deviate from the linear, $\dot\epsilon_0$-independent $\eta_E(t)$ versus t curves.

Ge-PEN and Sb-PEN. We see that Sb-PEN at 170 °C shows quite different behavior as compared to Ge-PEN at the same temperature, for which the critical strain ϵ_{η_E} remains almost constant around 1.5 and only slightly decreases in the region of small $\dot\epsilon_0$ (<0.01 s^{-1}), whereas for Sb-PEN at 170 °C ϵ_{η_E} decreases rapidly with decreasing $\dot\epsilon_0$. In the region of $\dot\epsilon_0$ below 0.1 s^{-1}, the behavior resembles that of Ge-PEN elongated at 190 °C.

Crystallization Behavior under Elongation. Figure 9 summarizes the TMDSC data of Sb-PEN elongated at 170 °C and Ge-PEN at 170 and 190 °C both

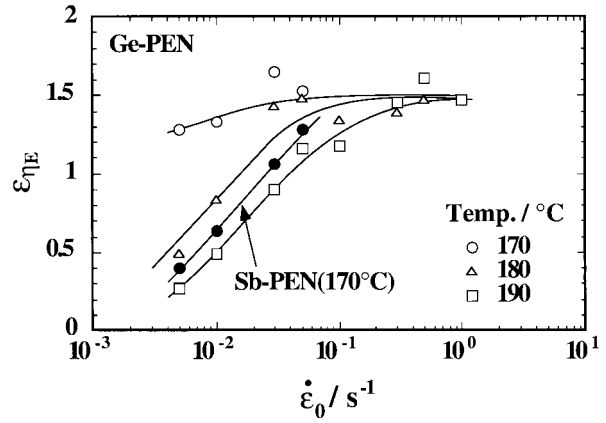

Figure 8. Strain rate $\dot{\epsilon}_0$-dependence of the *up-rising* Hencky strain $\epsilon_{\eta_E}(=\dot{\epsilon}_0 t_{\eta_E})$ for PENs between 170 and 190 °C.

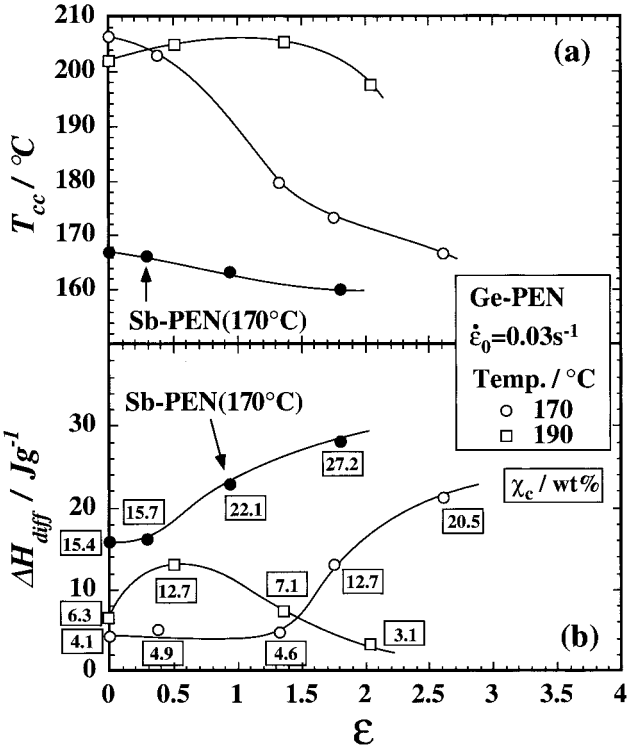

Figure 9. Plots of (a) cold crystallization temperature T_{cc} and (b) difference of the heat flow ΔH_{diff} for Sb-PEN elongated at 170 °C and Ge-PEN at 170 and 190 °C with $\dot{\epsilon}_0 = 0.03$ s^{-1}. The degree of % crystallinity χ_c of each specimen was shown with the number in the box.

with $\dot{\epsilon}_0 = 0.03$ s^{-1} to various extents of Hencky strain ϵ ($\equiv\dot{\epsilon}_0 t$). In Figure 9a are shown plots of cold crystallization temperature T_{cc} versus Hencky strain ϵ with T_{cc} being the exothermic (crystallization) peak temperature during a heating process of DSC, as seen in the lower temperature side of the main crystalline melting peak in the nonreversing and total heat flow profile (cf., Figure 1). On the other hand, Figure 9b shows the difference of the endothermic heat flow ΔH_{diff} ($=\Delta H_{rev} - \Delta H_{nonrev}$) between the reversing and nonreversing heat flow profiles. The ΔH_{diff} is expected to be proportional to the true degree of crystallinity χ_c (the number in the box attached to each symbol in wt % crystallinity) calculated from the TMDSC thermograms (cf., Figure 1). The T_{cc} represents the crystallization temperature of a specimen elongated to the given ϵ during the DSC run, while χ_c represents the crystallinity that existed in the stretched specimen before the DSC run.

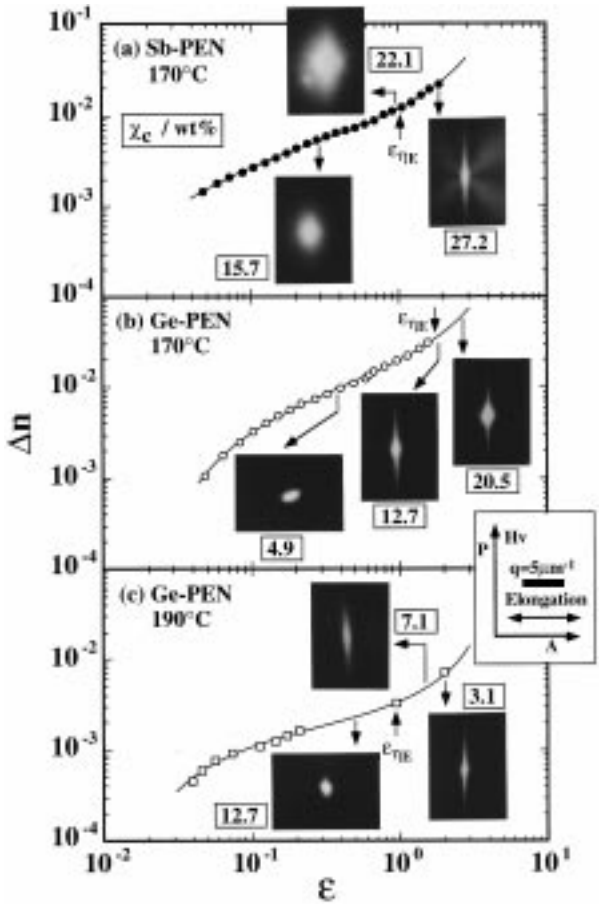

Figure 10. Double logarithmic plots of birefringence $\Delta n(t)$ versus Hencky strain ϵ ($=\dot{\epsilon}_0 t$) and the relevant LS patterns for (a) Sb-PEN elongated at 170 °C, (b) Ge-PEN at 170 °C, and (c) Ge-PEN at 190 °C with $\dot{\epsilon}_0 = 0.03$ s^{-1}. The degree of % crystallinity χ_c of each specimen was shown with the number in the box.

Changes in Birefringence and Scattering Patterns Induced by Elongation. Figure 10 shows birefringence $\Delta n(\epsilon)$ versus ϵ curves obtained at $\dot{\epsilon}_0 = 0.03$ s^{-1} with relevant Rayleigh scattering patterns for Sb-PEN elongated at 170 °C (a), and for Ge-PEN elongated at 170 (b) and at 190 °C (c). In the TMDSC data of Figure 9 we saw that, for Sb-PEN elongation at 170 °C, the χ_c starts at a relatively high level of ~15 wt % even in the early stage and reaches as high as $\chi_c = 22.1$ wt % at $\epsilon = 1.0$. For Sb-PEN at 170 °C the corresponding scattering pattern exhibits a strong anisotropy beyond $\epsilon = 0.6$ ($\cong\epsilon_{\Delta n}$, the critical *uprising* Hencky strain for birefringence at which the Δn versus tensile stress curve deviates from the linear dependence). The tendency of *strain-induced hardening* becomes prevailing at $\epsilon_{\eta_E} \cong 1.05$ (cf., Figure 8), where $\chi_c = \sim 22$ wt % and the scattering pattern becomes more and more intense and clear. Finally at $\epsilon = 1.85$, where $\chi_c \cong 27.2$ wt %, the LS pattern indicates the presence of rodlike crystalline aggregates,[21] suggesting that transformation and rearrangement from spherulites to new crystalline texture has taken place when Sb-PEN is elongated beyond ϵ_{η_E} ($\cong$1.05).

On the other hand, as seen in Figure 10b, Ge-PEN elongated at 170 °C up to $\epsilon \cong 0.37$ (where $\chi_c \cong 5$ wt %) exhibits a weak scattering pattern without any anisotropy. However, beyond $\epsilon > \epsilon_{\Delta n} \cong 1.65$, the LS pattern

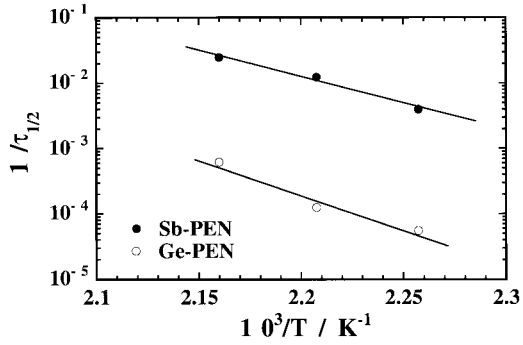

Figure 11. Temperature dependence of the reciprocal half-time of the spherulite growth $1/\tau_{1/2}$.

suddenly begins to exhibit strong streaks along the meridional direction perpendicular to the stretch direction, suggesting that strong molecular orientation has proceeded along the stretch direction in real space. Furthermore, at $\epsilon \cong 2.65$, the LS pattern exhibits strong streaks and χ_c jumps up to 20.5 wt %, where a significant *whitening* phenomenon was observed. The increasing of χ_c is an indication of the elongational flow-induced oriented crystallite formation. However, as opposed to the case for Ge-PET elongated at 110 °C with $\dot{\epsilon}_0 = 0.01$ s^{-1}, for which we saw a strong two-spot pattern in the direction parallel to the stretch direction,[3] we do not see such a pattern in Ge-PEN elongated at 170 °C. These results imply that the crystalline texture in Ge-PEN is disordered, as opposed to that in Ge-PET, in which an ordered pattern was observed.[3]

Now, Figure 10c shows similar data for Ge-PEN elongated at 190 °C with $\dot{\epsilon}_0 = 0.03$ s^{-1}. The crystallization behavior is entirely different from that of Ge-PEN elongated at 170 °C but resembles the behavior of Sb-PEN elongated at 170 °C. In Ge-PEN elongated at 190 °C as well as in Sb-PEN at 170 °C, the spherulite growth dominates especially in the specimen elongated with low $\dot{\epsilon}_0$ (<0.1 s^{-1}) and the critical Hencky strain ϵ_{η_E} is strongly dependent on $\dot{\epsilon}_0$, as seen in Figure 8.

In Ge-PEN elongated up to $\epsilon \cong 0.5$ at 190 °C, we observe a weak scattering pattern with slight anisotropy. Beyond $\epsilon > \epsilon_{\eta_E} \cong 0.9$, the LS pattern exhibits slightly smeared and broad streaks along the meridional direction perpendicular to the stretch direction, accompanying a decrease in χ_c from 12.7 to 7.1 wt %. Upon further elongating the specimen from $\epsilon = 1.4$ up to 2.05, the LS pattern becomes more desmeared and clear and χ_c further decreases from 7.1 to 3.1 wt %, where the elongated specimen is still transparent.

Discussion

Spherulite Growth under the Quiescent State. In Figures 4 and 5, we see that the spherulite growth rate under the quiescent state is roughly 40 times larger for Sb-PEN at 170 °C than that of Ge-PEN at 170 °C. We constructed Arrhenius plots of the reciprocal of the crystallization half-time, $1/\tau_{1/2}$, versus the reciprocal of the absolute temparature, $1/T$, for their spherulite growth behavior in the temperature range between 170 and 190 °C. Figure 11 compares the plots, $1/\tau_{1/2}$ versus $1/T$, for these PENs. We notice that the front factor for the plots for Sb-PEN is 40 times larger than that for Ge-PEN, but the slope that reflects the apparent activation energy for the spherulite growth is virtually the same (~5.2 kJ/mol). The result obviously implies that the number of nucleation sites is larger in Sb-PEN, but the spherulite growth mechanisms in the subsequent crystallization processes are virtually the same in both systems. Interestingly the tendency was the same for the Ge- and Sb-PET systems.[4]

Crystallization behavior under Elongation. As to the crystallization behavior under elongation shown in Figure 9, we notice for Sb-PEN elongated at 170 °C that T_{cc} slowly decreases and χ_c starts from a substantially high value of 15.4 wt % and steadily increases to 27.2% as ϵ is increased to 2. This behavior of T_{cc} and χ_c for Sb-PEN implies that the spherulites grow rapidly and keep growing even under elongation but eventually transform into deformed spherulites, as evidenced by the changes in the LS patterns seen in Figure 10a.

Figure 12 summarizes the LS pattern and a morphology model for Sb-PEN elongated at 170 °C with $\dot{\epsilon}_0 = 0.03$ s^{-1} up to $\epsilon = 1.8$ with χ_c reaching 27.2 wt %. Figure 12a is an enlarged version of the scattering pattern shown in Figure 10a, and Figure 12b is its schematic representation. The pattern consists of two parts: One is two split streaks inclined with an angle α, and the other is two diffuse lobes inclined with an angle β to the direction of elongation in real space. We see the two streaks with inclination α almost merge to one ($\alpha \cong 0$) and the lobes decrease their inclination β to 45°. Figure 12c depicts a morphology model that is composed of a rodlike entity of stacked lamellae with the rod axis orienting at an angle α and the lamellar axis at an angle β to the direction of elongation, as first proposed by Yau and Stein[22] some 30 years ago. The thin streaks may arise from the rods with inclination α ($\cong 0$) almost parallel, while the thick lobes may arise from the scattering from the stacked crystalline lamellae themselves with inclination β (~45°) to the direction of elongation.

On the other hand, the behavior of T_{cc} and χ_c for the elongation of Ge-PEN at 170 °C suggests the following: The rapid reduction in T_{cc} implies that the quenched PEN specimens once elongated at 170 °C to a high extent are more easily crystallizable during the DSC reheating process as compared to the unstretched specimen, while the behavior of χ_c suggests that, in the early stage of elongation, the orientation of the chain segments precedes and that, beyond $\epsilon \cong 1.35$, the oriented crystalline formation follows. In fact, as seen in Figure 10b, the scattering pattern from Ge-PEN elongated at 170 °C up to $\epsilon \cong 2.65$ yields a strong streak pattern, which is an indication of elongational flow-induced oriented crystallite formation. A similar scattering pattern was observed under a depolarized optical alignment of the Vv mode. These results imply that the crystalline texture grows normal to the oriented chain without regularity. For Ge-PEN elongated at 170 °C, the slow spherulite growth leads to the flow-induced oriented crystalline formation, in which the chains are first oriented along the direction parallel to the stretch direction and then lamellae develop in the direction perpendicular to the stretch direction, as depicted in Figure 13.

On the contrary, in the elongation of Ge-PEN at 190 °C, for which the spherulite growth rate is high but the grown spherulites are less well-organized and rather unstable, the behavior is quite peculiar: T_{cc} first slightly increases, passes a plateau around $\epsilon \cong 0.5-1.5$, and then decreases. Correspondingly, χ_c hits a maximum of 12.7 wt % at $\epsilon \cong 0.5$ and decreases to 3.1 wt % at $\epsilon \cong 2.05$, as seen in Figure 9. These results imply that once

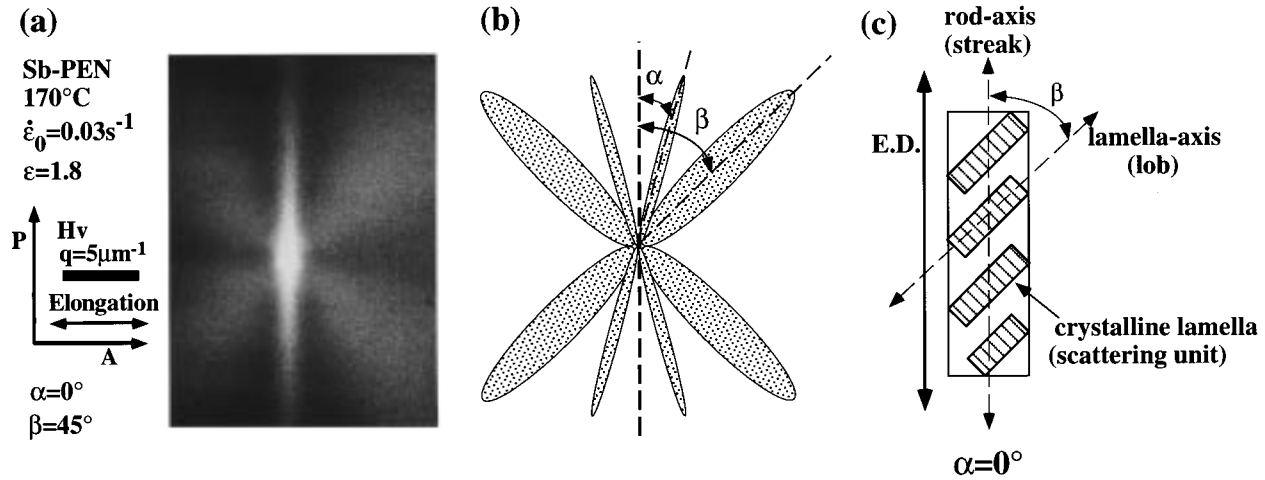

Figure 12. (a) Typical Hv scattering pattern for Sb-PEN elongated at 170 °C with $\dot{\epsilon}_0 = 0.03\ s^{-1}$ up to $\epsilon = 1.8$. (b) Its schematic representation and (c) a model describing the arrangement of rodlike texture with respect to the elongational direction (ED). The angles α and β are associated with the average orientation angle of the rods (the assembly of the lamellae) and that of the lamella axis, respectively, as depicted in the model.

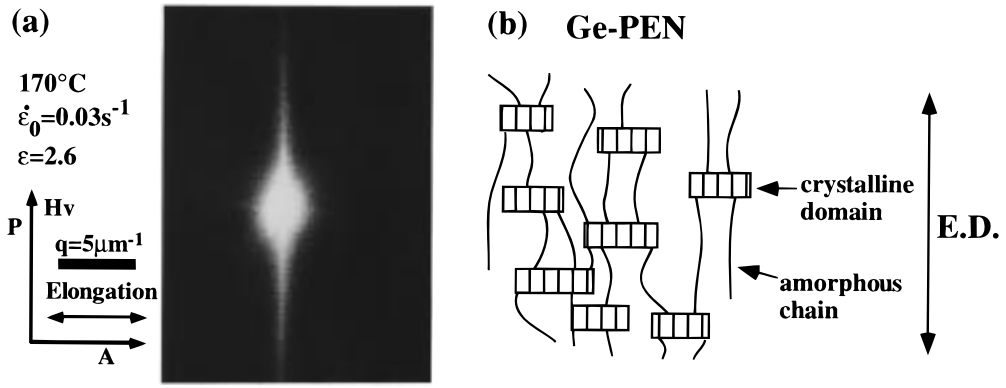

Figure 13. (a) Typical Hv scattering pattern for Ge-PEN elongated at 190 °C with $\dot{\epsilon}_0 = 0.03\ s^{-1}$ up to $\epsilon = 2.6$. (b) Model of the crystalline texture.

formed spherulites may melt upon stretching and the unfolded chains from the molten spherulites reorganize into extended-chain crystallites upon further stretching to a high extent. The LS patterns shown in Figure 10c are also indicative of such a transformation of the crystalline morphology.

Strain-Induced Hardening versus Crystallization Behavior. As discussed in our previous study on PET,[4] in the case of supercooled PEN elongation, the spherulite growth is also a key factor governing the elongational rheology. Generally spherulite growth leads to an enhancement in σ and thus in $\eta_E(\dot{\epsilon}_0;t)$ to an extent larger than that expected from the viscoelastic stress contribution. For Sb-PEN at 170 °C and Ge-PEN at 190 °C, in which spherulite growth was rapid (cf., Figure 4), we recognize that the critical Hencky strain ϵ_{η_E} ($\cong\dot{\epsilon}_0 t_{\eta_E}$) for the onset of strain-induced hardening is strongly $\dot{\epsilon}_0$-dependent. We thus examine here the strain-induced hardening behavior of PEN relative to the overall rate of crystallization that can be estimated via LS analysis under the quiescent state.

Using the reciprocal of *crystallization half-time*, $1/\tau_{1/2}$, as defined in Figure 5 for the overall crystallization rate, we reconstructed *reduced* plots of $\epsilon_{\eta E}$ versus $\dot{\epsilon}_0/(1/\tau_{1/2})$ from the ϵ_{η_E} versus $\dot{\epsilon}_0$ data of Figure 8 taken at different temperatures from 170 to 190 °C. The results are shown in Figure 14, in which the broken line is a reproduction of the reduced curve for Ge-PET elongated with various $\dot{\epsilon}_0$ in the temperature range from 110 to 130 °C.

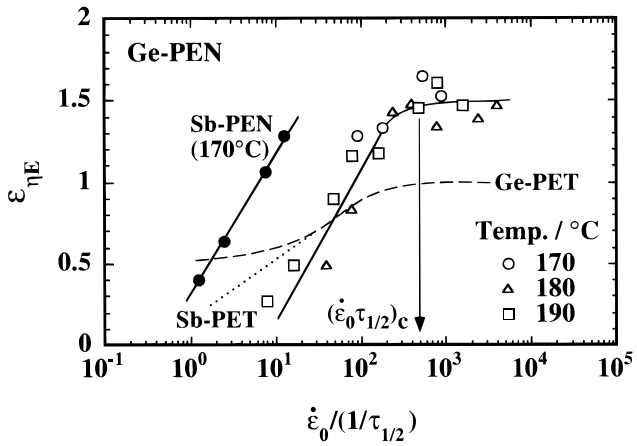

Figure 14. Reduced plots of ϵ_{η_E} versus $(\dot{\epsilon}_0 \cdot \tau_{1/2})$ for Sb-PEN and Ge-PEN elongated at various temperatures. The arrow indicates the critical (dimensionless) Hencky strain $(\dot{\epsilon}_0 \cdot \tau_{1/2})_c$ ($\cong$500). The broken and dotted lines indicate the reduced curves for Ge-PET and Sb-PET,[4] respectively.

We see that for Ge-PEN all the data nicely conform to the *reduced* curve with $\epsilon_{\eta_E} \cong 1.5$ for the dimensionless Hencky strain $\dot{\epsilon}_0 \cdot \tau_{1/2} > 500$, whereas the ϵ_{η_E} approaches zero as $\dot{\epsilon}_0 \cdot \tau_{1/2}$ is decreased well below 500. The estimated value of $(\dot{\epsilon}_0 \cdot \tau_{1/2})_c$ is thus $\cong$500. In the elongation of Ge-PEN with a high $\dot{\epsilon}_0 \cdot \tau_{1/2}$ (>500), elongational flow-induced oriented crystallite formation overwhelms, and otherwise the spherulite growth dominates the *strain-*

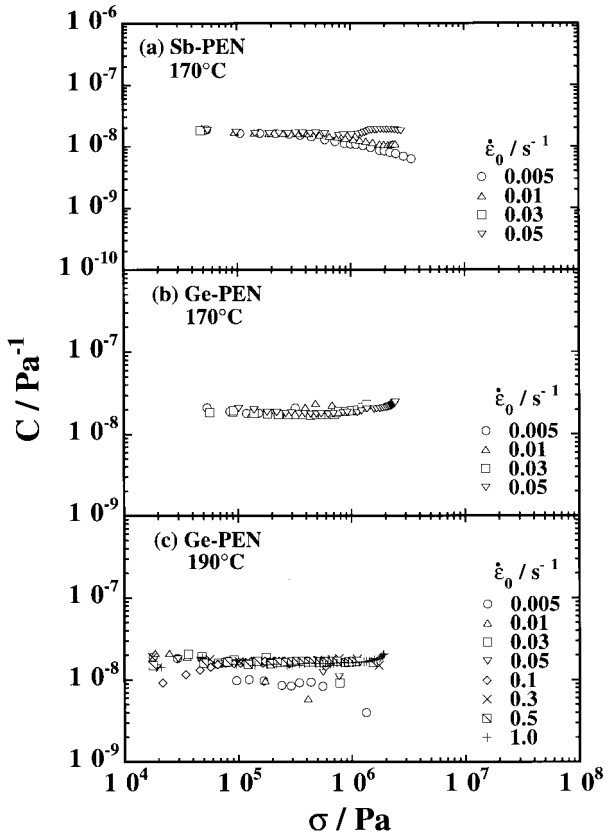

Figure 15. Double logarithmic plots of the stress optical coefficient $C = \Delta n/\sigma$ versus the tensile stress σ for (a) Sb-PEN elongated at 170 °C, (b) Ge-PEN at 170 °C, and (c) Ge-PEN at 190 °C with various strain rates $\dot{\epsilon}_0 = 0.005-1.0$ s^{-1}.

induced hardening behavior. In Ge-PEN, the value of $(\dot{\epsilon}_0 \cdot \tau_{1/2})_c$ is five times larger than that of Ge-PET elongation,[4] implying that the orientation of the rigid naphthalene rings is more difficult.

On the other hand, for Sb-PEN elongated at 170 °C we could not attain a high enough $\dot{\epsilon}_0 \cdot \tau_{1/2}$ where the elongational flow-induced oriented crystallite formation might overwhelm. Even in the elongation with low $\dot{\epsilon}_0 \cdot \tau_{1/2}$ (<10), the ϵ_{η_E} steadily decreases with decreasing $\dot{\epsilon}_0 \cdot \tau_{1/2}$, eventually approaching zero. This result may be an indication that although the spherulite growth rate is high, less stable spherulites in Sb-PEN may be easily deformed even in the early stage of elongation at low $\dot{\epsilon}_0 \cdot \tau_{1/2}$. The Rayleigh scattering profiles also reveal this feature to be the case, as discussed above.

Thus the $(\dot{\epsilon}_0 \cdot \tau_{1/2})_c$ is important in optimizing blow-molding conditions of PEN resins to obtain a transparent material containing the least amount of spherulites. Through these approaches of evaluating $(\dot{\epsilon}_0 \cdot \tau_{1/2})_c$, we may propose an optimum processing condition for blow-molding process of not only PEN resins of different grades but also other semicrystalline polymer resins such as metallocene-catalyzed polyolefins.

Stress Optical Rule for PEN under Elongation. For uniaxial elongation of a polymer melt the stress optical rule[23,24] simply reads

$$\Delta n = C \cdot \sigma \tag{3}$$

The stress optical coefficient $C = \Delta n/\sigma$, first given by Treloar *et al.*[25,26] for rubber elasticity, is supposed to be independent of time t, strain ϵ, tensile stress σ, or strain rate $\dot{\epsilon}_0$. Figure 15 compares the C versus σ curves for the supercooled PEN liquids: Figure 15a is for Sb-PEN elongated at 170 °C with varying $\dot{\epsilon}_0$ from 0.005 to 0.05 s^{-1}, Figure 15b is for Ge-PEN elongated at 170 °C within the same $\dot{\epsilon}_0$ range, and Figure 15c is for Ge-PEN at 190 °C with $\dot{\epsilon}_0$ from 0.005 to 1.0 s^{-1}.

For Sb-PEN, the value of C is constant ($\cong 1.80 \times 10^{-8}$ Pa^{-1}) in the early stage up to $\sigma \cong 0.4$ MPa, beyond which especially those elongated with low strain rates ($\dot{\epsilon}_0 <$ 0.01 s^{-1}) deviate downward. On the other hand, for Ge-PEN elongated at 170 °C with $\dot{\epsilon}_0$ from 0.005 to 0.05 s^{-1}, the C is nearly constant ($\cong 1.80 \times 10^{-8}$ Pa^{-1}, in agreement with that for Sb-PEN elongated at 170 °C) up to $\sigma \cong 1$ MPa, beyond which, however, upward deviation is seen. For Ge-PEN elongated at 190 °C, we see that C is also essentially constant, again in agreement with those for other PENs, but when the specimen is elongated with low strain rates ($\dot{\epsilon}_0 < 0.01$ s^{-1}), the value of C steadily deviates downward from the very beginning of elongation.

The downward deviation of C appears to always take place for PENs where spherulite growth is very rapid. This result might reflect the fact that the tensile stress increases but the birefringence hardly develops in the course of spherulite formation in the early stage of elongation, because optically symmetric spherulites may hardly contribute to the birefringence unless they have been significantly deformed. In contrast, for Ge-PEN elongated at 170 °C we see upward deviation of C in the late stage of elongation beyond ϵ_{η_E}, in which flow-induced oriented crystallite formation is prevailing rather than spherulite growth. We thus speculate that the excess Δn or C may presumably have arisen from the increasing orientation of crystalline lamellae along the stretch direction during the late stage of elongation. The upward deviation of C may happen even in Ge-PEN at 190 °C with a rapid spherulite growth rate especially when they are elongated with high strain rates $\dot{\epsilon}_0$ (>0.1 s^{-1}). Under such a condition the spherulite may be deformed and eventually transform into oriented crystallites.

Conclusions

We compared the elongational flow-induced crystallization behavior of rapidly crystallizable Sb-PEN with that of Ge-PEN in the temperature range where the spherulite growth rate is highly temperature-dependent. In Sb-PEN during the elongation at 170 °C, rapid growth of spherulites with low stability dominated in the early stage, and later transformation to a new crystalline texture, that is, the rod-like structure, occurred.

In the case of slowly crystallizable Ge-PEN elongated at 170 °C, however, flow-induced orientation of the chain segments preceded until a critical Hencky strain of $\epsilon_{\eta_E} \cong 2.65$ was reached, where oriented crystalline formation became prevailing, as revealed by TMDSC and the LS patterns. On the other hand, for Ge-PEN elongated at a temperature in the range from 180 to 190 °C with low strain rates $\dot{\epsilon}_0$ (<0.01 s^{-1}), where spherulite growth is substantial, the crystallization leads to *strain-induced hardening* and the subsequent reduction in C reflects a strong enhancement in σ but a rather weak enhancement in Δn due to the spherulite formation which contributes to σ but not much to Δn.

In the elongational flow of supercooled crystalline polymer liquids, obviously two mechanisms are competing, that is, the flow-induced oriented crystalline forma-

tion and the spherulite growth. Which one of the mechanisms overwhelms the rheology and birefringence is governed by whether the *dimensionless reduced strain rate* $\dot{\epsilon}\cdot\tau_{1/2}$ is above or below a certain critical value ($\cong$500 if $\tau_{1/2}$ is used as a measure for the overall crystallization rate). Another important factor governing the crystallization behavior is the stability or the deformability of the spherulites grown in the early stage. If the grown spherulites are unstable, they eventually undergo deformation and transformation into flow-induced oriented crystallites when stretched with high strain rates.

Acknowledgment. We wish to thank Dr. S. Irie of Teijin Ltd. for providing PEN samples with different crystallization habits.

References and Notes

(1) Kotaka, T.; Kojima, A.; Okamoto, M. *Rheol. Acta* **1997**, *36*, 646.
(2) Okamoto, M.; Kubo, H.; Kotaka, T. *Polymer* **1998**, *39*, 3153.
(3) Kubo, H.; Sato, H.; Okamoto, M.; Kotaka, T. *Polymer* **1998**, *39*, 501.
(4) Kubo, H.; Okamoto, M.; Kotaka, T. *Polymer*, in press.
(5) Jabarin, S. A. *Polym. Eng. Sci.* **1992**, *32*, 1341.
(6) Salem, D. R. *Polymer* **1994**, *35*, 771.
(7) Lorentz, G.; Tassin, J. F. *Polymer* **1994**, *35*, 3200.
(8) Ouchi, I.; Noda, H. *Sen-i Gakkaishi* **1973**, *29*, 405.
(9) Nakamae, K.; Nishino, T.; Tada, K.; Kanamoto, T.; Ito, M. *Polymer* **1993**, *34*, 3322.
(10) Murakami, S.; Nishikawa, Y.; Tsuji, M.; Kawaguchi, A.; Kohjiya, S.; Cakmak, M. *Polymer* **1995**, *36*, 291.
(11) Murakami, S.; Yamakawa, M.; Tsuji, M.; Kawaguchi, A.; Kohjiya, S. *Polymer* **1996**, *37*, 3945.
(12) Tate, S.; Watanabe, Y.; Chiba, A. *Polymer* **1993**, *34*, 4974.
(13) Meissner, J.; Hostettler, J. *Rheol. Acta* **1994**, *33*, 1.
(14) Wunderlich, B.; Jin, Y.; Boller, A. *Thermochim. Acta* **1994**, *238*, 277.
(15) Cheng, S. Z. D.; Wunderlich, B. *Macromolecules* **1988**, *21*, 789.
(16) Okamoto, M.; Inoue, T. *Polymer* **1995**, *36*, 2739.
(17) Okamoto, M.; Shinoda, Y.; Kinami, N.; Okuyama, T. *J. Appl. Polym. Sci.* **1995**, *57*, 1055.
(18) Koberstein, J.; Russel, T. P.; Stein, R. S. *J. Polym. Sci., Polym. Phys. Ed.* **1979**, *17*, 1719.
(19) Lee, C. H.; Saito, H.; Inoue, T. *Macromolecules* **1993**, *26*, 6566.
(20) Lee, C. H.; Saito, H.; Inoue, T.; Nojima, S. *Macromolecules* **1996**, *29*, 7034.
(21) Rhodes, M. B.; Stein, R. S. *J. Polym. Sci.* **1969**, *A2*, 7, 1539.
(22) Yau, W.; Stein, R. S. *J. Polym. Sci.* **1968**, *A2-6*, 1.
(23) Janeschitz-Kriegel, H. *Polymer Melt Rheology and Flow Birefringence*; Springer Verlag: Berlin, 1983.
(24) Doi, M.; Edwards, S. F. *The Theory of Polymer Dynamics*; Clarendon Press: Oxford, 1986; pp 221−222.
(25) Treloar, L. R. G. In *Die Physik Der Hochpolymeren*; Stuart, H. A., Ed.; Springer-Verlag: Berlin, 1956; Chapter 4.
(26) Treloar, L. R. G. *The Physics of Rubber Elasticity*, 3rd ed.; Clarendon Press: Oxford, 1975.

MA971713D